Cross-section measurements to low-lying excited final states in the ^{24}Mg$(\alpha, p)^{27}$Al$^*(\gamma)$ reaction as an energy source for x-ray bursts

T. Ahn,[1,2,*] S. Aguilar,[1,2] R. J. deBoer,[1,2] D. W. Bardayan,[1,2] A. Boeltzig,[1,2] C. R. Brune,[3] S. P. Burcher,[4] K. Y. Chae,[5] S. L. Henderson,[1,2] R. K. Grzywacz,[4] K. L. Jones,[4] J. M. Kovoor,[4] K. T. Macon,[1,2] K. Manukyan,[1] S. Mosby,[6] P. D. O'Malley,[1] M. Renaud,[1,7] K. Smith,[4,†] C. Thornsberry,[4] B. Vande Kolk,[1,2] and M. Wiescher[1,2]

[1]*Physics Department, University of Notre Dame, 225 Nieuwland Science Hall, Notre Dame, Indiana 46556, USA*
[2]*The Joint Institute for Nuclear Astrophysics, University of Notre Dame, Notre Dame, Indiana 46556, USA*
[3]*Edwards Accelerator Laboratory, Department of Physics and Astronomy, Ohio University, Athens, Ohio 45701, USA*
[4]*Department of Physics and Astronomy, University of Tennessee, Knoxville, Tennessee 37996, USA*
[5]*Department of Physics, Sunkyunkwan University, Suwon 16419, South Korea*
[6]*LANSCE Weapons Physics (P-27), Los Alamos National Laboratory, Los Alamos, New Mexico 87545, USA*
[7]*KU Leuven, Instituut voor Kern- en Stralingsfysica, 3001 Leuven, Belgium*

(Received 19 December 2019; accepted 25 August 2020; published 22 September 2020)

Energy production in Type Ia x-ray bursts depends on a number of nuclear reactions that become efficient in a hot environment (up to 2 GK). Model sensitivity studies have been performed in an effort to better identify the reactions that have the largest effect, but these efforts are hampered by the high level of complexity of the astrophysical model and large nuclear physics uncertainties. In a recent study, the ^{24}Mg$(\alpha, p)^{27}$Al reaction was found to significantly affect the energy generation in x-ray bursts. This manuscript reports the first study of the ^{24}Mg$(\alpha, p_{1,2}\gamma)^{27}$Al reaction at energies relevant for x-ray bursts. The branches to the ^{27}Al excited states increase to a small degree the estimates of the total astrophysical ^{24}Mg$(\alpha, p)^{27}$Al reaction rate.

DOI: 10.1103/PhysRevC.102.035805

I. INTRODUCTION

The modeling of Type Ia x-ray-burst light curves provides a direct test for our understanding of the dynamics of x-ray binaries and the underlying nuclear processes that drive them [1]. Due to the high temperatures reached in x-ray bursts in the 1 to 2 GK range, many nuclear reactions can participate in the energy generation and nucleosynthesis, making these environments very challenging to model. Because of this, a sensitivity study by Parikh *et al.* [2] used several different models that had a wide range of temperature-density profiles, initial compositions, and burst duration. Using these different studies, they identified the reactions that had the most significant impact on energy generation and nucleosynthesis. For their sensitivity study K04-B2, which used the model of Koike *et al.* [3] for a long burst duration, it was found that the ^{24}Mg$(\alpha, p)^{27}$Al reaction rate had a significant impact on the total nuclear energy when increased by 20%, the upper limit of the reaction's quoted uncertainty [4]. Further, based on the REACLIB compilation [5], it is interesting to note that over the higher temperatures accessed by x-ray bursts, the rate of the ^{24}Mg$(\alpha, p)^{27}$Al reaction does overtake the more well-studied ^{24}Mg$(\alpha, \gamma)^{28}$Si reaction rate. ^{24}Mg can be produced from ^{20}Ne α-capture reactions in the 1.0–1.5 MeV α-energy range [6] and the ^{24}Mg$(\alpha, \gamma)^{28}$Si reaction was cited as strongly contributing to the reaction flow for a different multizone x-ray-burst sensitivity study [7]. Due to the comparable reaction rate for the ^{24}Mg$(\alpha, p)^{27}$Al reaction near the peak temperature regime of x-ray bursts, further study of these α-induced reactions on ^{24}Mg are needed.

The rate of the ^{24}Mg$(\alpha, p)^{27}$Al reaction, having a Q value of $Q = -1.601$ MeV (α-particle separation energy $S_\alpha = 9.984$ MeV and proton separation energy $S_p = 11.585$ MeV), has been previously estimated solely on the basis of detailed balance using measurements of narrow resonance strengths from the ^{27}Al$(p, \alpha)^{24}$Mg reaction as compiled in Endt [8]. In fact, the ground-state ^{24}Mg$(\alpha, p_0)^{27}$Al reaction and its inverse reaction was used to validate the use of detailed balance to test time-reversal symmetry [9,10]. Based on the past reaction-rate studies, the ground-state branch of the ^{24}Mg$(\alpha, p)^{27}$Al reaction rate has been recently evaluated in Refs. [11–14]. However, while the ground-state portion of the reaction dominates at low temperatures, the population of excited final states in ^{27}Al ($E_x = 0.844$ and 1.014 MeV) at higher temperatures could enhance the rate compared to these previous estimates. It should also be noted that the ^{24}Mg $+\alpha$ reaction can only populate natural parity states in the ^{28}Si compound system. Because these reaction channels cannot be constrained by detailed balance using the reverse reaction due to the branches to the excited states of the final nucleus ^{27}Al, these reactions must be studied directly.

Past measurements of the ^{24}Mg$(\alpha, p)^{27}$Al reaction are very limited, although there have been a number of ^{24}Mg $+\alpha$ reactions studied including a thick-target γ-ray

*Corresponding author: tan.ahn@nd.edu
†Present address: Los Alamos National Laboratory, Los Alamos, NM 87545, USA.

measurement [15], and a number of ^{24}Mg$(\alpha,\gamma)^{28}$Si measurements [16–19]. Measurements of elastic scattering on ^{24}Mg and natural magnesium have been measured by Cseh *et al.* [20] and Cheng *et al.* [21], respectively. The only detailed study of the ^{24}Mg$(\alpha,p)^{27}$Al reaction is that of Kaufmann *et al.* [22] in 1952. This early data lacks an absolute scale for the cross section and measurements were limited to a single angle of observation. Further, only the ground-state transition, the ^{24}Mg$(\alpha,p_0)^{27}$Al reaction, was observed. The ^{24}Mg$(\alpha,p_{1,2})^{27}$Al* reactions are heavily suppressed due to the Coulomb barrier at low energies. These reactions are at least an order of magnitude smaller than the ^{24}Mg$(\alpha,p_0)^{27}$Al ground-state reaction at the energies measured by Kaufmann *et al.* [22], making the excited-state reactions close to or below the threshold of detection for that measurement.

To measure the cross sections of the ^{24}Mg$(\alpha,p)^{27}$Al reaction to the two dominant final excited states at $E_x = 0.844$ and 1.014 MeV over the energy range of interest in ^{27}Al, the method of secondary γ-ray spectroscopy has been used. Both of these ^{27}Al excited states decay via γ-ray emission with nearly 100% probability to the ground state [23]. Therefore, observation of the secondary γ rays at $E_\gamma = 0.844$ and 1.014 MeV can be used to accurately measure the ^{24}Mg$(\alpha,p_1)^{27}$Al and ^{24}Mg$(\alpha,p_2)^{27}$Al reaction channels without the need for γ-ray feeding corrections. It is energetically possible to populate higher-lying final states [$E_x(^{27}\text{Al}) = 2.212$, 2.835, 2.982, and 3.004 MeV] over some of the measured energy range. Very weak yields were observed only from the γ ray at 2.212 MeV (see Fig. 2), which has no reported feeding into the lower-energy excited states [23]. The method of secondary γ-ray detection is advantageous over direct particle detection in this circumstance as it eliminates the very large rate from ^{24}Mg$(\alpha,\alpha)^{24}$Mg elastic scattering allowing for the use of higher beam intensities.

Our experimental procedure is described in Sec. II. The extraction of yields from the observed γ-ray spectra is described in Sec. III, and the contribution to the reaction rate is determined in Sec. IV. Conclusions and a look to future work are given in Sec. V.

II. EXPERIMENTAL SETUP AND PROCEDURE

Experimental measurements were performed at the Nuclear Science Laboratory at the University of Notre Dame [24]. The 5-MeV Sta. ANA accelerator was used to produce a beam of doubly ionized ^{4}He^{2+} ranging in laboratory energy from $E_\alpha = 4.0$ to 5.4 MeV, which corresponds to a center-of-mass energy of $E_{\text{c.m.}} = 3.4$ to 4.6 MeV and a ^{28}Si excitation energy of $E_x(^{28}\text{Si}) = 13.4$ to 14.6 MeV. The α beam was impinged on a thin magnesium target with a thickness of 34.9(34) μg/cm^2 that was produced by evaporating isotopically enriched, 99.91(1)% in ^{24}Mg, magnesium metal onto a tantalum backing 0.2 mm thick. The target thickness was determined by the observed energy loss for the narrow resonance at $E_\alpha = 4.309$ MeV ($E_{\text{c.m.}} = 3.693$ MeV, $E_x = 13.677$ MeV) in the ^{24}Mg$(\alpha,p_2)^{27}$Al reaction. The target was produced and was kept under an argon atmosphere during transportation between the evaporator and the target station to minimize oxidation. The target was kept under rough vacuum in the target station for a few hours before being transferred to the beam line where it was kept under high vacuum. When under beam bombardment, the target backing was water cooled and the beam was rastered over the target surface to reduce target degradation. A copper pipe was positioned a few millimeters in front of the target inside the beam pipe and was biased to -300 V to suppress secondary electrons from the target. In addition, the copper pipe was cooled with liquid nitrogen, greatly reducing carbon buildup on the target. Beam intensities throughout the experiment were typically $\approx$10 eμA. Repeated thick-target resonance scans of the strong narrow resonance observed at $E_\alpha = 4.309$ MeV in the ^{24}Mg$(\alpha,p_2\gamma)^{27}$Al reaction showed no appreciable change in target thickness over the course of the experimental measurements. Beam current was monitored via an electrically isolated target holder as the beam was fully stopped in the tantalum target backing. The reproduciblity of the beam current integration was determined to be accurate to 3% through repeated testing.

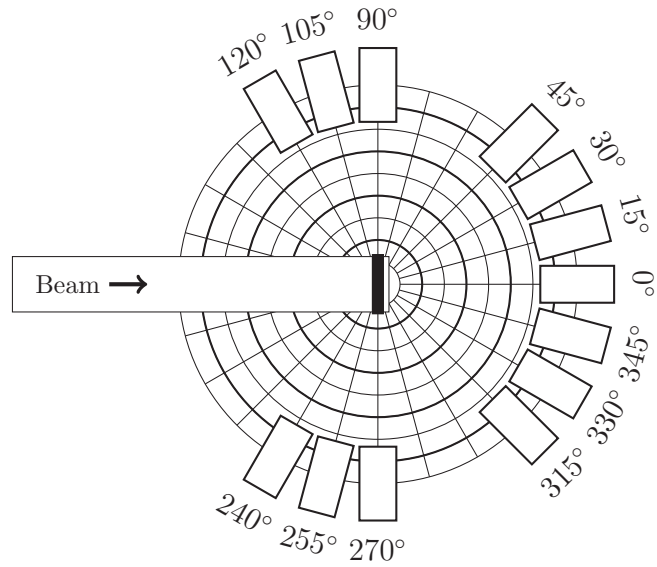

FIG. 1. A schematic of the experimental setup. The detectors are of type $LaBr_3$ from the HAGRiD array, which were used to measure angular distributions of secondary γ rays from the ^{24}Mg$(\alpha,p_{1,2}\gamma)^{27}$Al reaction. The water-cooled target is indicated by the black rectangle in the center of the HAGRiD array.

Secondary γ rays were detected using an array of 13, 2 in. $\times$ 2 in. diameter, $LaBr_3$ detectors from the Hybrid Array of Gamma Ray Detectors (HAGRiD) [25]. The detectors were placed approximately 12 in. from the center of the target position from 0 to 120°. Because secondary γ-ray angular distributions are symmetric about both 180° and 90° relative to the direction of the beam [26], the setup effectively measures the angular distribution between 0 and 90° in 15° increments. The target and detector setup is shown schematically in Fig. 1. To reduce the effects of misalignment of the beam spot, detectors were placed at symmetric positions at either side of the target, except for the detector at 0°. Two sets of detectors were also placed at backward angles for reduced γ-ray attenuation from the target holder. A digital data acquisition system was

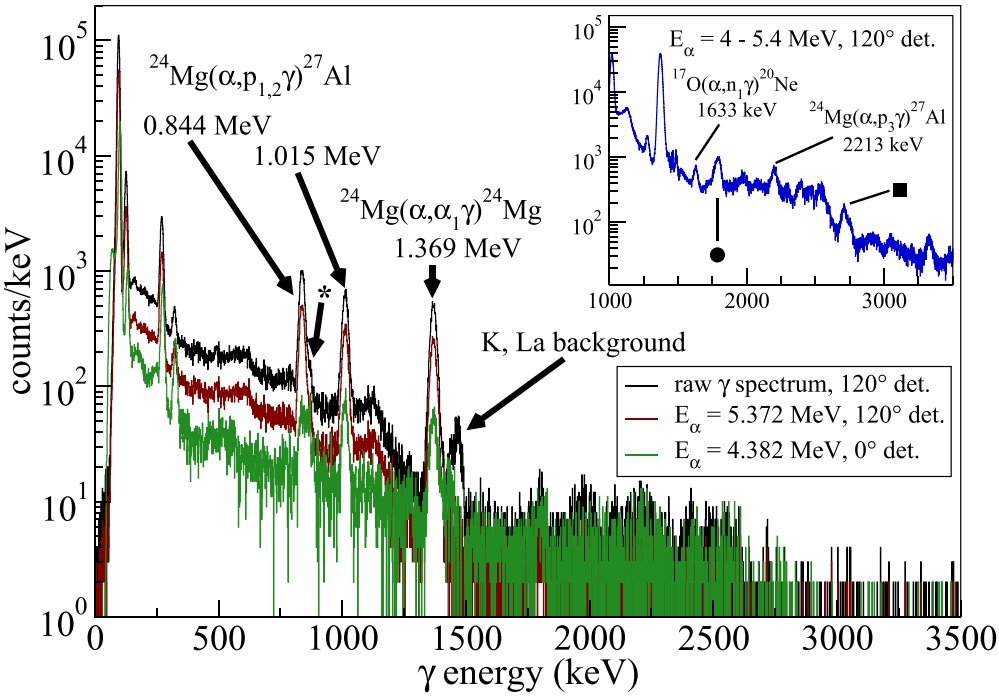

FIG. 2. The raw γ-ray energy spectrum for one of the 120° $LaBr_3$ detectors for $E_\alpha = 5.372$ MeV is shown. The background-subtracted spectrum is directly under the raw γ spectrum. Under this spectrum, a third γ spectrum is shown for a different energy and angle ($E_\alpha = 4.382$ MeV, 0°). Secondary γ-ray peaks from the $^{24}Mg(\alpha, p_1)^{27}Al$, $^{24}Mg(\alpha, p_2)^{27}Al$, and $^{24}Mg(\alpha, \alpha_1)^{24}Mg$ reactions are indicated as well as a beam-induced background line (indicated by *) and room and intrinsic $LaBr_3$ background lines. A background-subtracted sum spectrum for the 120° detector for the energy range $E_\alpha = 4$–5.4 MeV is shown (inset) and the γ decay for the $^{24}Mg(\alpha, p_3\gamma)^{27}Al$ and $^{17}O(\alpha, n_1\gamma)^{20}Ne$ reactions from target oxidation can be seen. The circle ($E_\gamma = 1.778$ MeV) indicates a peak that is likely from the $^{24}Mg(\alpha, \gamma)^{28}Si$ reaction and the square ($E_\gamma = 2.788$ MeV) indicates a peak that is possibly from the $^{18}O(\alpha, n_3)^{21}Ne$ reaction.

used to record the γ rays triggering on each channel individually. The integrated charge on the target was also recorded with each run.

III. ANALYSIS

Because the γ-ray lines of interest are all below 1.3 MeV, the efficiency calibration of the $LaBr_3$ detectors was performed using calibrated ^{137}Cs and ^{60}Co sources. In addition, a background run was recorded immediately after the in-beam runs that was used to subtract the intrinsic background from the $LaBr_3$ detectors and the room background from the measured spectra.

Beam-induced background could also be present from inelastic scattering on any ^{27}Al that might be present. Several other secondary γ-ray experiments have been performed recently on the same beam line using the same target configuration and no γ-ray lines have been observed at the energies of interest. Background runs were also performed on a tantalum blank at a few energies and no observable yield was found. In addition, a long room background run was taken at the end of the experiment and no activation of beam-line components or target was observed.

Secondary γ-ray yields were extracted from the $LaBr_3$ energy spectra for γ rays at $E_\gamma = 0.844$ and 1.014 MeV [23,27], which correspond to γ-ray decays from the first two excited states of ^{27}Al directly to the ground state for the reactions $^{24}Mg(\alpha, p_1\gamma)^{27}Al$ and $^{24}Mg(\alpha, p_2\gamma)^{27}Al$, respectively. In Fig. 2, the peaks corresponding to these γ decays can be seen in the raw γ-ray spectrum for the $\theta_{lab} = 120°$ detector for the α energy $E_\alpha = 5.372$ MeV. In addition, the $E_\gamma = 1.369$ MeV γ ray from the $^{24}Mg(\alpha, \alpha_1)^{24}Mg$ reaction was observed to be strong. It was also energetically possible to populate the higher-lying states in ^{27}Al at $E_x(^{27}Al) = 2.212$, 2.735, 2.982, and 3.004 MeV as well as the states at $E_x(^{24}Mg) = 4.123$, 4.238, and 5.235 MeV in ^{24}Mg. It is expected that the cross sections to populate these excited states will be strongly suppressed due to the Coulomb barrier, and only weak yields from the 2.212-MeV γ ray were observed, which can be seen in the inset background-subtracted sum spectrum in Fig. 2. Additional peaks in this energy region can be seen. There is a γ-ray line at $E_\gamma = 1.633$ MeV, which is from the $^{17}O(\alpha, n_3)^{20}Ne$ reaction; a γ-ray line at $E_\gamma = 1.778$ MeV, which is likely from the $^{24}Mg(\alpha, \gamma)^{28}Si$ reaction; and a γ-ray line at ($E_\gamma = 2.788$ MeV), which may possibly be from the $^{18}O(\alpha, n_3)^{21}Ne$ reaction. The yield from the 1.633-MeV peak was later used to determine the oxygen content of the target.

For each experimental energy spectrum from the $LaBr_3$ detectors, the room background spectrum, normalized by the run time, was subtracted. In Fig. 2, it can be seen that the intrinsic $LaBr_3$ and natural potassium γ-ray peaks are absent in the background-subtracted spectrum. The gains of some of the $LaBr_3$ detectors shifted on the order of 1×10^{-3} to 2×10^{-3} over the course of the experiment, which translates to 1–2 keV in energy for the γ rays of interest. The γ-ray energies for each run were gain matched so the contribution

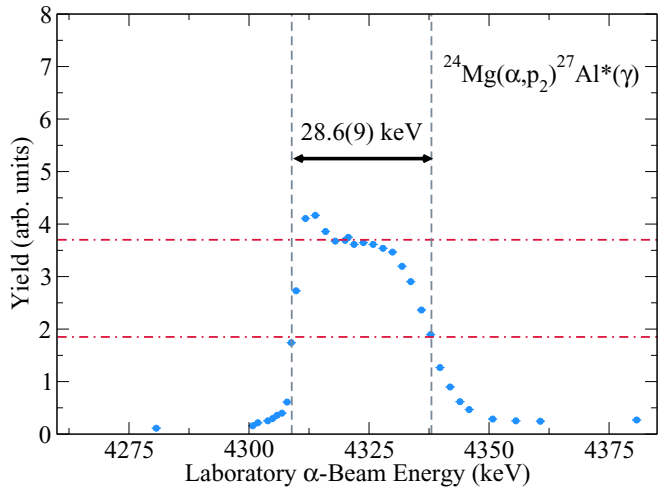

FIG. 3. The thick-target profile of the narrow resonance at $E_\alpha = 4.309$ MeV ($E_{\text{c.m.}} = 3.693$ MeV, $E_x = 13.677$ MeV) in the $^{24}\text{Mg}(\alpha, p_2\gamma)^{27}\text{Al}$ reaction.

of the gain shifts to the total detector resolution is estimated to be much smaller than 1 keV. For some detectors at the same angle, there were measurable differences of up to 7% in the γ-ray yields. These differences are within reason due to slight misalignments of the beam and these differences should be averaged when summing the yields of each detector. The peaks in the background-subtracted spectra were fit with a linear background plus Gaussian function to obtain the final yields. For the 0.844-MeV γ-ray, there was an in-beam γ-ray contaminant that overlapped it that was not part of the room background spectrum. It is likely that this is a 0.868-MeV γ ray that comes from the 2_1^+ level of ^{16}O. Although this contaminant peak was overlapping our 0.844-MeV peak, it was sufficiently separated that we were able to cleanly fit both peaks with a constrained double-Gaussian fit plus linear background fit.

The differential cross section is expected to be composed of a mix of narrow and broad resonances given the properties of the nuclear structure in this region reported by Nelson *et al.* [28,29]. Because the energy loss through the target ($22 < \Delta E_\alpha < 29$ keV) was often much greater than the widths of the underlying resonances, extraction of the absolute differential cross section would require a deconvolution, which would have to rely heavily on resonance information from other measurements and sometimes require structure information that is unknown. Because the reaction rates can be determined from the normalized thick-target yields, deconvolution was not necessary.

The overall systematic uncertainty is dominated by the uncertainty in the target thickness and stoichiometry due to oxidation of the target. The α-particle energy loss through the target was determined using the narrow resonance ($\Gamma = 1.9$ keV [28,29]) at $E_\alpha = 4.309$ MeV ($E_{\text{c.m.}} = 3.693$ MeV, $E_x = 13.677$ MeV) in the $^{24}\text{Mg}(\alpha, p_2\gamma)^{27}\text{Al}$ reaction. The thick-target profile of this narrow resonance is shown in Fig. 3. An energy loss of 28.6(9) keV was observed in the laboratory frame.

The stoichiometry of the target was determined using the secondary γ-ray yield from the $^{17}\text{O}(\alpha, n_1\gamma)^{20}\text{Ne}$ reaction ($E_\gamma = 1.634$ keV), which was observed as a background in the measured spectra over the strong resonance in the reaction at $E_\alpha = 5.0$ MeV. The total cross section of the $^{17}\text{O}(\alpha, n)^{20}\text{Ne}$ reaction has been measured by Bair and Haas [30] and it is expected that the first excited state should dominate the total cross section over this energy range [31]. This has been verified by new measurements at the University of Notre Dame [32]. Given the dominating 25% systematic uncertainty in the $^{17}\text{O}(\alpha, n)^{20}\text{Ne}$ cross section [30], the uncertainty in the natural isotopic abundance of oxygen isotopes of 3%, and the 10% uncertainty in the experimental γ-ray yields over the resonance, the effective oxygen thickness was found to be 8(2) $\mu\text{g/cm}^2$.

Using the partial stopping powers from SRIM [33] for oxygen and magnesium (both having an uncertainty of 5%) and the energy loss observed for the narrow resonance in the $^{24}\text{Mg}(\alpha, p_2\gamma)^{27}\text{Al}$ reaction at $E_\alpha = 4.309$ MeV (3% uncertainty), a thickness of 34.9 ± 3.4 $\mu\text{g/cm}^2$ was determined for the ^{24}Mg in the target. The uncertainty in the efficiency was determined to be 5% using calibrated ^{60}Co and ^{137}Cs sources. This leads to an overall systematic uncertainty of 11%. The α-particle beam has a resolution of approximately 0.5 keV and an uncertainty of ± 3 keV over the energy range of the measurements.

The normalized differential yields for the 13 LaBr_3 detectors were determined using

$$\frac{dY}{d\Omega} = \frac{dA/d\Omega}{N_t N_b \epsilon(E_\gamma)}, \tag{1}$$

where $dA/d\Omega$ are the integrated yields of the γ-ray peaks extracted from the LaBr_3 spectra, N_t are the number of target atoms, N_b are the number of beam particles impinged on the target, and $\epsilon(E_\gamma)$ is the efficiency for a γ ray of energy E_γ. As secondary γ-ray angular distributions are also symmetric about 90°, the backward-angle measurements can be treated as their forward-angle equivalents. This results in a measurement at seven unique angles from 0° to 90° in 15° increments. A GEANT4 [34] simulation was performed to determine the Q coefficients [35] for the detection setup up to a relative orbital angular momentum of 4. Because of the far geometry and small detector size, the coefficients were found to deviate from unity by less than 1%.

The normalized differential thick-target yields were then integrated over the angular range using a Legendre polynomial fit,

$$\frac{dY}{d\Omega} = \sum_{l=0,\text{even}}^{l_{\max}} a_l P_l(\cos\theta_\gamma), \tag{2}$$

where $P_l(\cos\theta_\gamma)$ are the Legendre polynomials of order l, $l_{\max}$ is the maximum order used, and a_l are the angular distribution coefficients that are treated as free parameters in the fitting. As angular distributions for secondary γ rays are symmetric about 90°, only even order coefficients are possible. An $l_{\max} = 4$ was chosen and the Legendre coefficients were fit using a least-squared minimization. Equation (2) is linear in the fit coefficients a_l, and therefore these least-squared coefficients

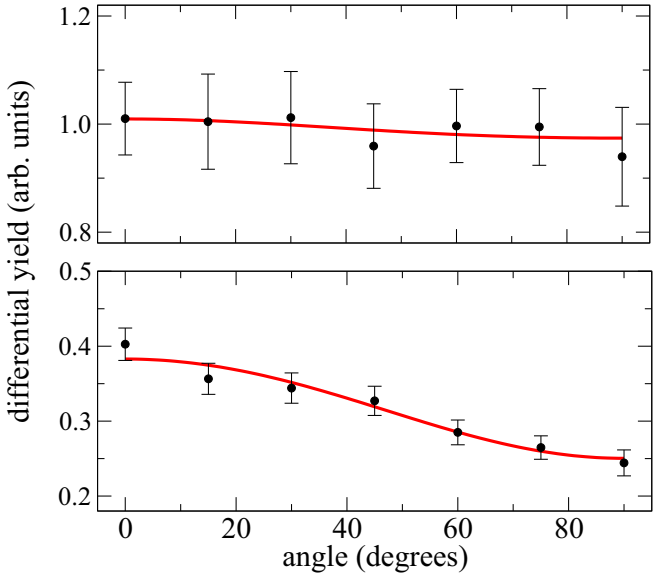

FIG. 4. Angular distributions of γ rays at $E_\alpha = 4.822$ MeV ($E_{\text{c.m.}} = 4.132$ MeV, $E_x = 14.117$ MeV) for the $^{24}\text{Mg}(\alpha, p_1)^{27}\text{Al}$ and $^{24}\text{Mg}(\alpha, p_2)^{27}\text{Al}$ reactions are shown in the top and bottom plots, respectively. The solid red line shows the Legendre polynomial fit.

were found directly by employing matrix inversion [36]. An example of an angular distribution fit for the measurement at $E_\alpha = 4.822$ MeV ($E_{\text{c.m.}} = 4.132$ MeV, $E_x = 14.117$ MeV) is shown in the top and bottom panels in Fig. 4 for the (α, p_1) and (α, p_2) reactions, respectively.

The normalized angular distribution coefficients a_2/a_0 and a_4/a_0 are plotted in Figs. 5 and 6 for the two reaction channels. The $^{24}\text{Mg}(\alpha, p_1\gamma)^{27}\text{Al}$ reaction shows only very small deviations from isotropy, while the $^{24}\text{Mg}(\alpha, p_2\gamma)^{27}\text{Al}$ reaction shows more deviation, manifesting as statistically significant deviations of the a_2/a_0 coefficient from zero. Both reactions show no significant a_4/a_0 contributions.

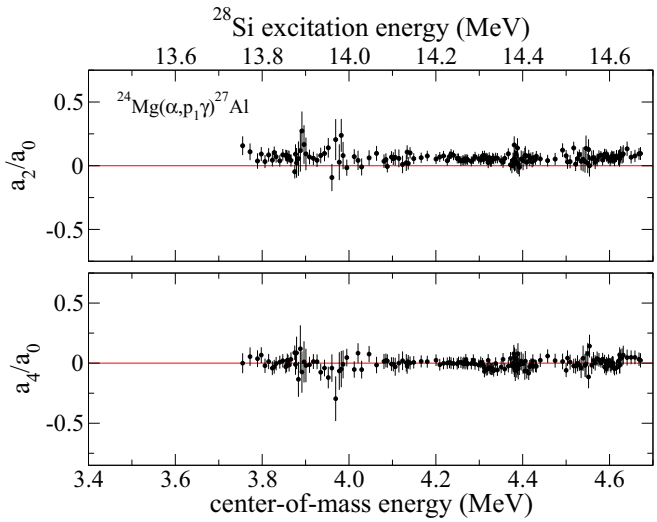

FIG. 5. Plot of the a_2/a_0 coefficients (top) and a_4/a_0 (bottom) coefficients for the $^{24}\text{Mg}(\alpha, p_1\gamma)^{27}\text{Al}$ reaction.

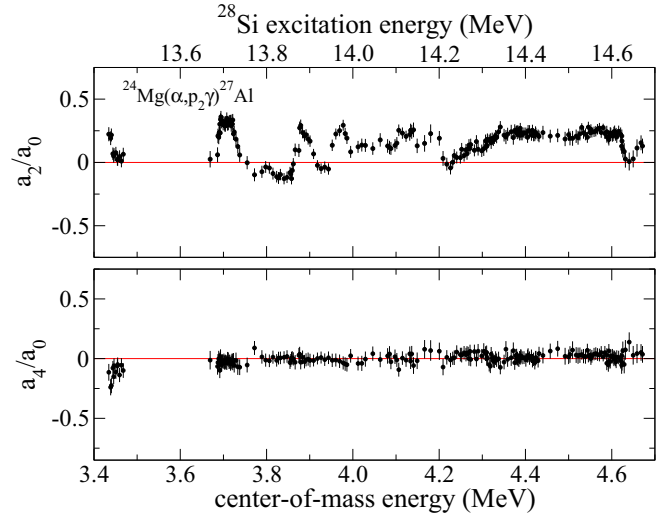

FIG. 6. Plot of the a_2/a_0 coefficients (top) and the a_4/a_0 coefficients (bottom) for the $^{24}\text{Mg}(\alpha, p_2\gamma)^{27}\text{Al}$ reaction.

The angle-integrated yields are deduced from the a_0 coefficient as $Y = 4\pi a_0$. The angle-integrated yields are shown in Fig. 7 where the horizontal axis gives the center-of-mass energy for the measured data point. Due to our finite experimental energy resolution, which is mainly due to energy loss through the target, the vertical axis scale is in arbitrary units but would correspond to units of barns in regions where the widths of resonances are large compared to the energy loss through the target. A number of resonances can be seen including a broad resonance in the (α, p_1) reaction at 4.32 MeV of center-of-mass energy ($E_x = 14.30$ MeV). Several of the observed resonances correspond to levels observed in $^{27}\text{Al}+p$ reactions. The most comprehensive measurement over this energy range is reported in Nelson *et al.* [28,29]. In that work, cross sections were reported for the $^{27}\text{Al}(p, p_0)^{27}\text{Al}$, $^{27}\text{Al}(p, p_1)^{27}\text{Al}^*$, $^{27}\text{Al}(p, p_2)^{27}\text{Al}^*$, $^{27}\text{Al}(p, \alpha_0)^{24}\text{Mg}$, and $^{27}\text{Al}(p, \alpha_1)^{24}\text{Mg}^*$ reactions, and a simultaneous R-matrix fit was performed, extracting partial widths.

To illustrate the correspondence between the resonances observed here and those observed in the $^{27}\text{Al}+p$ reactions, the partial widths from Nelson *et al.* [28,29] were used to perform an R-matrix calculation using the code AZURE2 [37,38] for the $^{24}\text{Mg}(\alpha, p_1)^{27}\text{Al}$ and $^{24}\text{Mg}(\alpha, p_2)^{27}\text{Al}$ reactions. The calculations are shown as a dashed line in Fig. 7, where the R-matrix cross section has been convoluted with the resolution of the present experiment. The R-matrix calculation shows correspondence between many of the resonances observed in our measurement and the previously reported levels, but several levels not observed in Nelson *et al.* [28,29] are seen in our data. These levels were observed in the $^{27}\text{Al}(p, \gamma)^{28}\text{Si}$ reaction [8] except for one possible level we have observed at $E_x = 14.235$ MeV in the $^{24}\text{Mg}(\alpha, p_1)^{27}\text{Al}$ channel. In particular, the resonances above 4 MeV in center-of-mass energy for the (α, p_1) reaction channel do not appear in the R-matrix calculation. These levels likely did not appear in the data of Nelson *et al.* [28,29] for two reasons. First because Nelson *et al.* [28,29] populated resonances using the $^{27}\text{Al}+p$ entrance pair, levels with weak ground-state proton partial widths (Γ_{p_0})

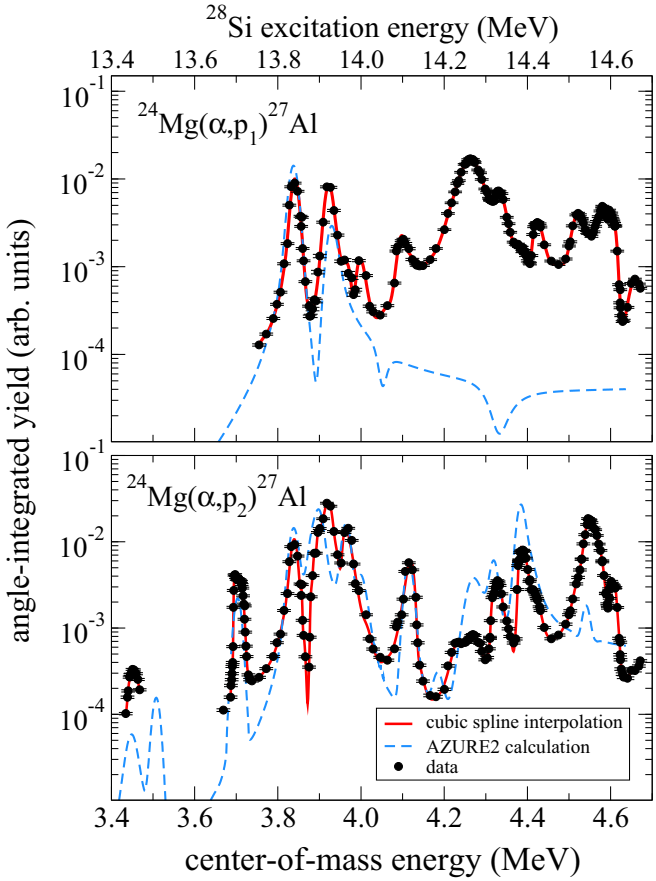

FIG. 7. Integrated angular yields for the ^{24}Mg$(\alpha, p_1)^{27}$Al and ^{24}Mg$(\alpha, p_2)^{27}$Al reactions. The solid line shows the interpolation of the data using a cubic spline. The vertical axis scale is in arbitrary units but corresponds to units of barns in regions where the underlying cross section varies slowly with energy. The dashed blue line shows an estimate of the cross section based on the experimental results of Nelson *et al.* [28,29], convoluted with the resolution of the present measurements, calculated with the *R*-matrix program AZURE2.

will not be observed, while in the present work levels with large ground-state α partial widths Γ_{α_0} are favored. Second, due to their experimental conditions, Nelson *et al.* [28,29] were only sensitive to strongly populated levels in the (p, p_1) and (p, p_2) reactions, whereas the present measurements have significantly greater sensitivity.

Because a comprehensive *R*-matrix fit of all reaction channels is beyond the scope of the present work, the angle-integrated yields were fit with a cubic spline, which was used to interpolate the (α, p_1) and (α, p_2) yields to calculate these reaction channels' contributions to the total ^{24}Mg$(\alpha, p)^{27}$Al reaction rate as described in Sec. IV. The differential cross-section data and resulting angle-integrated data are given in the Supplemental Material [39].

IV. REACTION RATE

Sensitivity studies for x-ray bursts in Parikh *et al.* [2] calculated the ^{24}Mg$(\alpha, p)^{27}$Al rate incorrectly by using the inverse rate of the ^{27}Al$(p, \alpha)^{24}$Mg reaction rate of Iliadis *et al.* [4] (updated in Longland *et al.* [11] and Iliadis *et al.* [12–14]). However, detailed balance is only applicable if the final states in both entrance and exit channels are the same and no distinction was made between the resonance contributions that populate the ground-state ^{27}Al$(p, \alpha_0)^{24}$Mg reaction and the excited-state ^{27}Al$(p, \alpha_1)^{24}$Mg reaction in those works. To investigate this discrepancy, the contribution of the ^{27}Al$(p, \alpha_1)^{24}$Mg component to the total ^{27}Al$(p, \alpha)^{24}$Mg reaction rate has been recalculated using the branching ratios given in Endt [8]. Despite there being many more levels observed in the (p, α_1) reaction, the majority of them are weak compared to those observed in the (p, α_0) reaction, and the (p, α_1) reaction channel was found to contribute less than 3% to the total reaction rate over the entire temperature range of interest. Therefore, because this contribution is much smaller than the uncertainty of the reaction rate, the rate of Iliadis *et al.* [4] is for all practical purposes equivalent to the ground-state portion of the ^{24}Mg$(\alpha, p_0)^{27}$Al rate and is treated as such for further calculations in this work.

TABLE I. Reaction rates for the (α, p_1) and (α, p_2) channels. The uncertainties in these reaction rates are ±16%.

	$N_A\langle\sigma v\rangle$ (cm^3 mol^{-1} s^{-1})	
T (GK)	(α, p_1)	(α, p_2)
1	1.46×10^{-12}	7.43×10^{-12}
1.5	2.84×10^{-6}	8.60×10^{-6}
2	3.89×10^{-3}	9.60×10^{-3}
2.5	2.92×10^{-1}	6.28×10^{-1}
3	5.10×10^{0}	9.90×10^{0}
3.5	3.85×10^{1}	6.94×10^{1}
4	1.73×10^{2}	2.93×10^{2}
4.5	5.47×10^{2}	8.86×10^{2}
5	1.36×10^{3}	2.12×10^{3}
6	5.14×10^{3}	7.60×10^{3}
7	1.29×10^{4}	1.84×10^{4}
8	2.51×10^{4}	3.47×10^{4}
9	4.14×10^{4}	5.60×10^{4}
10	6.07×10^{4}	8.08×10^{4}

To calculate the total ^{24}Mg$(\alpha, p)^{27}$Al reaction rate, the additional contributions from the ^{24}Mg$(\alpha, p_1)^{27}$Al and ^{24}Mg$(\alpha, p_2)^{27}$Al reaction channels are required. These contributions have not been included in previous rate calculations because no data have been available. Using the measurements of the present work, these contributions were calculated by integration of the cubic-spline fit of the angle-integrated yields determined in Sec. III, where the reaction rate is given by

$$N_A\langle\sigma v\rangle = \left(\frac{8}{\pi\mu}\right)^{\frac{1}{2}} \frac{1}{(kT)^{\frac{3}{2}}} \int E\sigma(E) e^{-E/kT} dE, \qquad (3)$$

where N_A is Avogadro's number, E is the center-of-mass energy, k is Boltzmann's constant, and T is the temperature of the environment. The reaction rates were calculated from 1 to 10 GK, covering the energy range of interest for x-ray bursts, and are listed in Table I. Including the other systematic uncertainties due to beam-integration and target-thickness

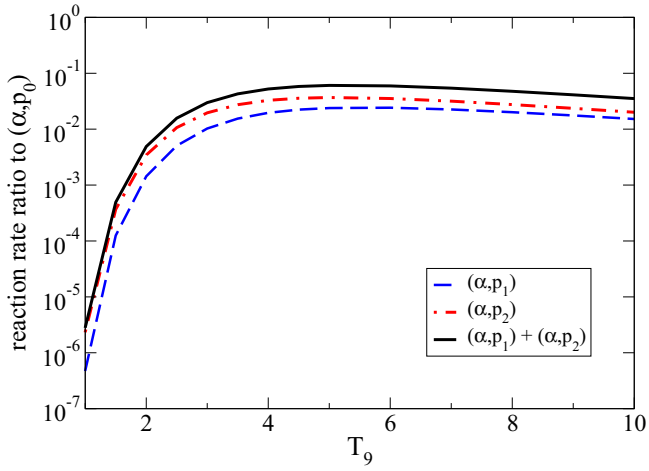

FIG. 8. The ratio of ^{24}Mg$(\alpha, p_1)^{27}$Al (dashed line), ^{24}Mg$(\alpha, p_2)^{27}$Al (dashed-dotted line), and the sum of the two (solid line) to the ^{24}Mg$(\alpha, p)^{27}$Al reaction rate from Refs. [11–14].

uncertainties, our total reaction rate uncertainty is 16%, which is dominated by the target-thickness uncertainty of 15%. These contributions are compared to the ^{24}Mg$(\alpha, p_0)^{27}$Al reaction rate used by Parikh *et al.* [2] (calculated by Longland *et al.* [11] and Iliadis *et al.* [12–14] as discussed above). Values for the rates were obtained using the REACLIB data base [5].

The ratios of the rate contributions from the (α, p_1) and (α, p_2) reactions to what is effectively the (α, p_0) reaction rate of Iliadis *et al.* [4] are shown in Fig. 8. For temperatures below 2 GK, the contribution of the excited-state reactions is relatively small. The sum of both excited-state reactions increases to 0.49% at 2 GK. The individual (α, p_1) and (α, p_2) ratios at 2 GK have values of 0.14% and 0.35%, respectively. Above 2 GK, these ratios continue to increase their maximum values of 2.4% and 3.7%, respectively, giving a total contribution of 6.1% of the (α, p_0) reaction rate at 5 GK. For temperatures higher than 5 GK, the ratios slowly decrease in magnitude.

For x-ray-burst temperatures reaching values around 2 GK, the contribution of the excited-state reactions is relatively small at 0.49%. This shows that the original reaction-rate calculation based on detailed balance of the ^{27}Al$(\alpha, p)^{24}$Mg reaction that considers only the ground-state reaction is a good approximation and modifications to it are marginal. It should be noted that one could not assume a small excited-state reaction contribution *a priori*. The existence of one or multiple strong resonances at low energy in the excited-state reactions could have contributed significantly for x-ray-burst temperatures, but we have ruled out this possibility for resonances in the 3.4 to 4.6 MeV center-of-mass energy range. In addition, for astrophysical events that reach higher temperatures, such as core-collapse supernovas, the excited state contributions may reach 6%.

V. SUMMARY AND OUTLOOK

Measurements of the ^{24}Mg$(\alpha, p_{1,2}\gamma)^{27}$Al reaction have been made for the first time covering the energy range relevant for x-ray-burst energy production. The reaction rate was determined by direct integration of the observed secondary γ-ray yields obtained from the HAGRiD detector array, and the component of the reaction rate due to the population of excited states in ^{27}Al was determined. This contribution was found to be less than 0.49% of the total rate at temperatures below 2 GK, making these reaction channels negligible for x-ray-burst temperatures. However, at higher temperatures the contribution was found to be up to 6.1%. Although the excited-state contribution to x-ray-burst reaction rates were small, the excited-state contributions were not studied directly before, and therefore it was necessary to investigate the possibility low-energy resonances that could make a substantial contribution to the reaction rates. An analysis is under way to combine the present data with other reaction data that populate the ^{28}Si compound system in a global *R*-matrix calculation to obtain a more precise rate estimate for the ^{24}Mg$(\alpha, p)^{27}$Al reaction and to improve the description of the level structure over this energy region. This will allow us to gain a better understanding of the underlying level structure over this excitation energy range.

ACKNOWLEDGMENTS

This work was supported by the U.S. National Science Foundation under Grant No. PHY-1713857 and the U.S. Department of Energy under Grants No. DE-FG02-88ER40387, No. DE-NA0003883, and No. DE-FG02-96ER40963. This work was sponsored in part by the National Nuclear Security Administration under the Stewardship Science Academic Alliance program through DOE Cooperative Agreement No. DE-NA000213. The analysis utilized resources from the Notre Dame Center for Research Computing and was supported by the National Science Foundation through Grant No. PHY-0758100 and the Joint Institute for Nuclear Astrophysics through Grants No. PHY-0822648 and No. PHY-1430152 (JINA Center for the Evolution of the Elements). R.J.d.B. acknowledges useful discussions from the International Atomic Energy Agency "Consultants meetings about *R*-matrix codes for charged-particle reactions in the resolved resonance region." This work was also supported by National Research Foundation of Korea (NRF) grants funded by the South Korean government (Grants No. NRF-2019R1F1A1058370 and No. NRF-2016R1A5A1013277).

[1] W. H. G. Lewin, J. Van Paradijs, and R. E. Taam, Space Sci. Rev. **62**, 223 (1993).

[2] A. Parikh, J. José, F. Moreno, and C. Iliadis, Astrophys. J. Suppl. Ser. **178**, 110 (2008).

[3] O. Koike, M.-A. Hashimoto, R. Kuromizu, and S.-I. Fujimoto, Astrophys. J. **603**, 242 (2004).

[4] C. Iliadis, J. M. D'Auria, S. Starrfield, W. J. Thompson, and M. Wiescher, Astrophys. J. Suppl. Ser. **134**, 151 (2001).

[5] R. H. Cyburt, A. M. Amthor, R. Ferguson, Z. Meisel, K. Smith, S. Warren, A. Heger, R. D. Hoffman, T. Rauscher, A. Sakharuk, H. Schatz, F. K. Thielemann, and M. Wiescher, Astrophys. J. Suppl. Ser. **189**, 240 (2010).
[6] E. Strandberg, M. Beard, M. Couder, A. Couture, S. Falahat, J. Görres, P. J. LeBlanc, H. Y. Lee, S. O'Brien, A. Palumbo, E. Stech, W. P. Tan, C. Ugalde, M. Wiescher, H. Costantini, K. Scheller, M. Pignatari, R. Azuma, and L. Buchmann, Phys. Rev. C **77**, 055801 (2008).
[7] R. H. Cyburt, A. M. Amthor, A. Heger, E. Johnson, L. Keek, Z. Meisel, H. Schatz, and K. Smith, Astrophys. J. **830**, 55 (2016).
[8] P. Endt, Nucl. Phys. A **633**, 1 (1998).
[9] W. Von Witsch, A. Richter, and P. Von Brentano, Phys. Rev. **169**, 923 (1968).
[10] E. Blanke, H. Driller, W. Glöckle, H. Genz, A. Richter, and G. Schrieder, Phys. Rev. Lett. **51**, 355 (1983).
[11] R. Longland, C. Iliadis, A. E. Champagne, J. R. Newton, C. Ugalde, A. Coc, and R. Fitzgerald, Nucl. Phys. A **841**, 1 (2010).
[12] C. Iliadis, R. Longland, A. Champagne, A. Coc, and R. Fitzgerald, Nucl. Phys. A **841**, 31 (2010).
[13] C. Iliadis, R. Longland, A. Champagne, and A. Coc, Nucl. Phys. A **841**, 251 (2010).
[14] C. Iliadis, R. Longland, A. Champagne, and A. Coc, Nucl. Phys. A **841**, 323 (2010).
[15] R. K. Heaton, H. W. Lee, B. C. Robertson, E. B. Norman, K. T. Lesko, and B. Sur, Phys. Rev. C **56**, 922 (1997).
[16] J. A. Weinman, L. Meyer-Schützmeister, and L. L. Lee, Phys. Rev. **133**, B590 (1964).
[17] L. Meyer-Schützmeister, Z. Vager, R. Segel, and P. Singh, Nucl. Phys. A **108**, 180 (1968).
[18] E. Kuhlmann, K. A. Snover, G. Feldman, and M. Hindi, Phys. Rev. C **27**, 948 (1983).
[19] D. Bohle, K. Glasner, L. Ricken, and E. Kuhlmann, Z. Phys. A: At. Nucl. **318**, 339 (1984).
[20] J. Cseh, E. Koltay, Z. Máté, E. Somorjai, and L. Zolnai, Nucl. Phys. A **385**, 43 (1982).
[21] H.-S. Cheng, H. Shen, F. Yang, and J.-Y. Tang, Nucl. Instrum. Methods Phys. Res. Sect. B **85**, 47 (1994).
[22] S. G. Kaufmann, E. Goldberg, L. J. Koester, and F. P. Mooring, Phys. Rev. **88**, 673 (1952).
[23] M. S. Basunia, Nucl. Data Sheets **112**, 1875 (2011).
[24] Institute for Structure and Nuclear Astrophysics, University of Notre Dame, https://isnap.nd.edu, accessed: 2019-11-25.
[25] K. Smith, T. Baugher, S. Burcher, A. Carter, J. Cizewski, K. Chipps, M. Febbraro, R. Grzywacz, K. Jones, S. Munoz, S. Pain, S. Paulauskas, A. Ratkiewicz, K. Schmitt, C. Thornsberry, R. Toomey, D. Walter, and H. Willoughby, Nucl. Instrum. Methods Phys. Res. Sect. B **414**, 190 (2018).
[26] H. J. Rose and D. M. Brink, Rev. Mod. Phys. **39**, 306 (1967).
[27] R. Firestone, Nucl. Data Sheets **108**, 2319 (2007).
[28] R. O. Nelson, E. G. Bilpuch, C. R. Westerfeldt, and G. E. Mitchell, Phys. Rev. C **29**, 1656 (1984).
[29] R. O. Nelson, E. G. Bilpuch, C. R. Westerfeldt, and G. E. Michell, Phys. Rev. C **30**, 755 (1984).
[30] J. K. Bair and F. X. Haas, Phys. Rev. C **7**, 1356 (1973).
[31] P. Mohr, Phys. Rev. C **96**, 045808 (2017).
[32] K. Macon, A. Boeltzig, Y. Chen, M. Couder, R. deBoer, J. Görres, Q. Liu, L. Morales, C. Seymour, G. Seymour, B. V. Kolk, and M. Wiescher (unpublished).
[33] J. F. Ziegler, M. D. Ziegler, and J. P. Biersack, Nucl. Instrum. Methods Phys. Res. Sect. B **268**, 1818 (2010).
[34] J. Allison, K. Amako, J. Apostolakis, P. Arce, M. Asai, T. Aso, E. Bagli, A. Bagulya, S. Banerjee, G. Barrand *et al.*, Nucl. Instrum. Methods Phys. Res. Sect. A **835**, 186 (2016).
[35] M. E. Rose, Phys. Rev. **91**, 610 (1953).
[36] P. R. Bevington and D. K. Robinson, *Data Reduction and Error Analysis for the Physical Sciences,* 3rd ed. (McGraw-Hill, New York, 2003).
[37] R. E. Azuma, E. Uberseder, E. C. Simpson, C. R. Brune, H. Costantini, R. J. de Boer, J. Görres, M. Heil, P. J. LeBlanc, C. Ugalde, and M. Wiescher, Phys. Rev. C **81**, 045805 (2010).
[38] E. Uberseder and R. J. deBoer, `AZURE2` User Manual (2015), azure.nd.edu.
[39] See Supplemental Material at http://link.aps.org/supplemental/10.1103/PhysRevC.102.035805 for a tabulation of the experimental data from this work.